Scientific Research Publishing

Journal of Quantum Information Science, 2021, 11, 84-98
https://www.scirp.org/journal/jqis
ISSN Online: 2162-576X
ISSN Print: 2162-5751

Quantum Mechanical Calculations of High-T_c Fe-Superconductors

Ronald Columbié-Leyva[1*], Ulises Miranda[2], Alberto López-Vivas[1], Jacques Soullard[3], Ilya G. Kaplan[1]

[1]Instituto de Investigación en Materiales, National Autonomous University of Mexico, Ciudad de México, México
[2]Institute of Atomic Physics and Spectroscopy, University of Latvia, Riga, Latvia
[3]Instituto de Física, National Autonomous University of Mexico, Ciudad de México, México
Email: *naldor1401@gmail.com

How to cite this paper: Columbié-Leyva, R., Miranda, U., López-Vivas, A., Soullard, J. and Kaplan, I.G. (2021) Quantum Mechanical Calculations of High-Tc Fe-Superconductors. *Journal of Quantum Information Science*, **11**, 84-98.
https://doi.org/10.4236/jqis.2021.112007

Received: May 21, 2021
Accepted: June 22, 2021
Published: June 25, 2021

Abstract

In introduction we presented a short historical survey of the discovery of superconductivity (SC) up to the Fe-based materials that are not superconducting in a pure state. For this type of material, the transition to SC state occurs in presence of different dopants. Recently in the Fe-based materials at high pressures, the SC was obtained at room critical temperature. In this paper, we present the results of calculations of the isolated cluster representing infinitum crystal with Rh and Pd as dopants. All calculations are performed with the suite of programs Gaussian 16. The obtained results are compared with our previous results obtained for embedded cluster using Gaussian 09. In the case of embedded cluster our methodology of the Embedded Cluster Method at the MP2 electron correlation level was applied. In the NBO population analysis two main features are revealed: the independence of charge density transfer from the spin density transfer and, the presence of orbitals with electron density but without spin density. This is similar to the Anderson's spinless holon and confirms our conclusions in previous publications that the possible mechanism for superconductivity can be the RVB mechanism proposed by Anderson for high T_c superconductivity in cuprates.

Keywords

Superconductivity, Fe-Based Superconductors, Embedded Cluster Method, MP2 Method, NBO Analysis

1. Introduction

In 1911 Kamerlingh Onnes [1] discovered the superconductivity (SC) of the Hg (at critical T_c = 4.19 K), while he was doing his experiments on the resistivity of

gold and mercury wires at low temperature. At that time, Kamerlingh was the only one who could reach very low temperatures because he was the first who obtained the liquid helium. At that moment, a new state of the matter was discovered, the SC state. For explaining the mechanism of SC, it was required the creation of quantum mechanics (1925), see [2] [3] [4] [5] [6], the formulation of the Pauli Exclusion Principle (1925) [7] [8], the creation of quantum field theory (QFT) [9], and many other developments in quantum mechanics, before in 1957 Bardeen-Cooper-Schrieffer (BCS) [10] [11] formulated their famous microscopic theory of superconductivity.

The BCS theory was based on creation of Cooper pairs (pair of electrons that attract each other, instead of repelling, through the interaction with the lattice vibrations). Later on, Gor'kov [12] generated the microscopic formulation of the phenomenological macroscopic Ginzburg-Landau (G-L) theory [13] [14]. After, Eliashberg [15] created a new approach to the conventional superconductors, broadening the range of application of the BCS theory to systems with strong electron-phonon interaction.

For many years the critical temperature T_c was low, the maximum critical temperature was obtained for Nb3Sn, T_c = 18.5 K. In 1986 Bednorz and Müller [16] discovered the high T_c (~30 K) SC in the cuprates family. For $YBa_2Cu_3O_7$ the lowest T_c = 65 K [17] was obtained for zero pressure. As was shown in [18] [19] [20] for different materials, the increase of pressure leads to an increase of T_c.

One of the long-standing challenges was the observation of room-temperature SC. For many years numerous laboratories failed to increase T_c. The progress arises after Drozdov *et al.* [21] using high pressure obtained for sulfur hydride system a T_c = 203 K. At last, in 2020 Snider *et al.* [22] obtained the really room-temperature SC with the T_c = 287.7 K (15˚C) for a photochemically transformed carbonaceous sulfur hydride. They used the diamond anvil cell with a palladium thin film that assisted the synthesis by protecting the sputtered yttrium from oxidation and promoting subsequent hydrogenation. These types of materials are characterized by high frequencies vibration that increases the electron-phonon coupling, which is needed for high T_c phonon mediated SC, that is, for conventional SC.

The discovery in 2008 by Hosono and coworkers [23] [24] of the superconductivity in the $La[O_{(1-x)}\ F_x]FeAs$ with (x = 0.05 − 0.12) represented the rise of a new era with the family of high-T_c Fe-based superconductors (Fe-SC), which are also named as iron-based superconductors (IBSC). This family is composed by six groups of IBSC compounds [25]. Among them, the Ba-based crystals, $BaFe_2As_2$, are widely used [26]-[32]. They have a high-quality single crystal and are easily growing. It is very important that for this crystal it is easy to produce SC materials with a variety of chemical doping. It is for this material that the SC phase was first observed by Co substitution on the Fe site [27]. The parent compound is a paramagnetic semimetal, it turns into superconductor upon electron

doping by d-electrons atoms (substitution of Fe atoms by Co, Ni, Rh or Pd) or upon hole doping in the plane of the Ba atoms (e.g., substitution of Ba atoms by K).

IBSC materials where intensively studied by theorists, see [33]-[46] and references therein. It was shown that the IBSC material has a quite complicated band structure and several disconnected Fermi surfaces (FSs) [33] [34] [35]. According to these studies all five 3d orbitals of the Fe are involved in the formation of the FSs. IBSC belong to the broad category of strongly correlated superconductors such as heavy fermions and cuprates high-T_c SC, although the latter has rather different mechanism of SC. We recommend the readers the popular and comprehensive reviews by Norman [36] [37], Mazin [38], Wang and Lee [39], Chubukov [40], Kordyuk [41], Baquero [42] and Prosorov *et al.* [43].

From the first year of the discovery of the IBSC, it has been accepted that the superconductivity in these materials is non-conventional, presenting an anti-ferromagnetic (AFM) order. As was proposed by Mazin *et al.* [33] [34], these new superconducting materials tend to form AFM order, and the magnetism existing in the parent crystal at zero doping is suppressed by the AFM spin fluctuations, similar results were obtained also by Singh and Du [35]. The AFM spin fluctuations can induce s-wave pairing with sign change of the order parameter between the electron like FSs and hole like FSs, denoted as $s_{\pm}$. At the same time, Kuroki *et al.* [44] applied multiorbital random-phase approximation [45] to the model of five d-orbitals and obtained similar results as in [33] [35], but they also accepted the d-wave symmetry. Other types of symmetry have been proposed by Onari and Kontani [46], being d-wave symmetry, and also opposing to the $s_{\pm}$-wave symmetry [47].

The parent compound in IBSC can be considered as some kind of Mott insulator [48] [49] [50] [51] [52] and the physics of a Mott insulator may play an important role in the IBSC mechanism. From this model also follows the anti-ferromagnetism and $s_{\pm}$ pairing [48] [49] [50] [51] [52]. As was discussed in the review by Lee *et al.* [53], the Anderson resonating valence bond (RVB) theory, that was first proposed for cuprates, can be applied to the Mott insulating model naturally.

The RVB theory [54] for high T_c superconductors was proposed after the discovery of the cuprates. In this theory the antiferromagnetic lattice is melted into a spin-liquid phase composed by singlet pairs. When doping is applied, the singlets become charged giving rise to the superconducting state. This theory takes into account the separation between spin and charge, then the electronic excitation spectra can be presented as two different branches: charged spinless holons and chargeless spinons [55] [56].

In our previous publications devoted to IBSC [57] [58] [59], we performed the comparative studies of the electronic structure of the pure $Ba_4Fe_5As_8$ cluster and doped with substitutions of Fe atom by two pairs of dopants Co, Ni and Rh, Pd.

The Embedded Cluster Method at the Möller-Plesset second order electron correlation level (ECM-MP2) [60] [61] [62] was used and the detailed charge and spin distribution at the Natural Bond Orbital (NBO) analysis [63] [64] [65] was obtained. In these calculations, spinless electron on the 3d orbitals was obtained, pointing out on the Anderson RVB model as the possible mechanism for superconductivity for this new type of material.

In this article we study the electronic structure of the isolated Ba4Fe5As8 cluster doped by Rh and Pd using unrestricted Möller-Plesset second order (MP2) method. The presented results obtained by the GAUSSIAN 2016 A.03 [66] suite of programs and will be compared with our previous results performed also by GAUSIAN 2016 A.03 [62] but for the embedded cluster. We will analyze the energy difference between the isolated cluster and the embedded cluster and the NBO orbital population as well.

2. Methodology

The embedded cluster method at the Möller-Plesset second order electron correlation level (ECM-MP2) was used. The ECM-MP2 methodology includes two stages. At the first stage, the cluster representing the crystal is selected and the quantum-mechanical MP2 calculations are performed with the unrestricted Hartree-Fock (UHF) method, as the zero-order approximation. A detailed description of MP2 is given in Appendix 3 of book [67].

The complete structural information is taken from [26]. The selected cluster composed by 17 atoms is depicted on **Figure 1**. This selection must maintain the symmetry of the crystal. Since we study the influence of local effects in the electronic structure, we placed one of the Fe atoms, which will be substituted by dopants in the centre of the cluster.

At the second stage, the cluster is embedded in a background charges that reproduce the Madelung potential for the infinite crystal. Two conditions must be fulfilled: 1) the symmetry of the crystal must be preserved; 2) the cluster with the background charges must be neutral. The background charges are taken from our previous studies [57] [58]. Then the cluster with the background charges is calculated at the MP2 level. The charges are modified and the whole system is recalculated, repeating this process until self-consistency is achieved, see [60] [61].

The calculations are performed with the Gaussian 2016 A.03 suite of programs [66]. The triply split valence basis set is used (6-311G(d)) for Fe [68] [69] [70] and As [71] [72] [73] and all electrons are taken into account for both atoms. For heavier atoms, the relativistic Wood-Boring pseudopotential [74] [75] for the core electrons on Ba [76], Rh [77] and Pd [77] was used, and its associated basis sets were used for the valence electrons. The UHF calculations and then the MP2 calculations are performed using unrestricted HF results as initial guess. The electron and spin distribution are studied using the NBO analysis [63] [64] [65].

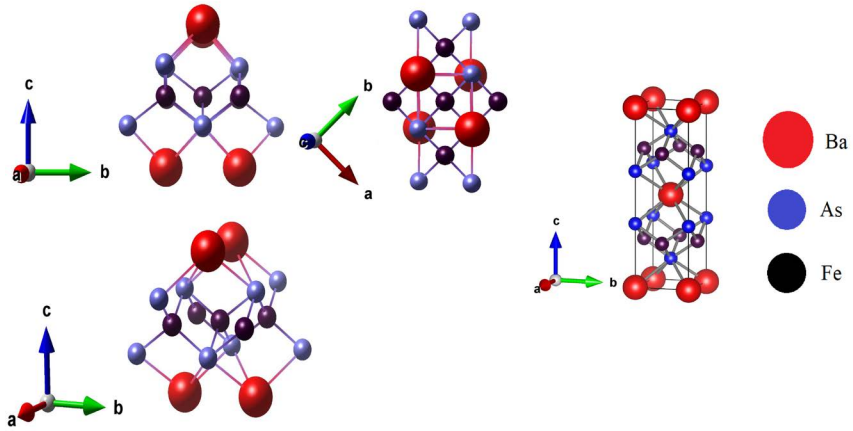

Figure 1. The cluster $Ba_4Fe_5As_8$ from different directions and the unit cell of studied crystal $BaFe_2As_2$ (right).

3. Results and Discussion

3.1. The Isolated and Embedded Cluster Energy and Its Dependence on the Multiplicity of the State

In Table 1 we present the energy and multiplicity for ground state of the pure and doped isolated cluster $Ba_4Fe_5As_8$ calculated by GAUSSIAN 2016 A.03 [66]. The multiplicity is defined as $M = 2S + 1$ where S is the total spin of the state. The eigenvalues of the S^2 operator, $S^2 = S(S + 1)$, which is used for checking the spin contamination of the state and the corrected spin contamination values are given in parenthesis. In our non-relativistic quantum-mechanic calculations, the operator S^2 commutes with the Hamiltonian that does not depend on the spin, therefore the spin S is a good quantum number.

The presented new results correspond to the isolated cluster. According to Table 1, for the pure cluster the energy diminishes till the multiplicity $M = 8$ and this was the reason for the calculation until $M = 10$, where the energy begins to increase. Thus, as follows from Table 1 the ground state in this case corresponds to multiplicity $M = 8$ ($S = 7/2$). The ground state for the cluster doped by Rh is the singlet state, which is a non-magnetic state. However, we are interested in magnetic states. Thus, we should analyse states beginning from triplet state, $S = 1$. It follows that the ground state has $M = 5$ ($S = 2$). In the case of Pd doping, a large spin contamination is observed for two multiplicities $M = 2$ and $M = 4$, therefore these results should not be trusted. Nevertheless, the most probable that the ground state for the Pd doping has $M = 6$ ($S = 5/2$).

In Table 1, it is also presented our old results from [59], where also unrestricted MP2 calculations were used, but for the embedded cluster. In this case, for the pure cluster the ground state has $M = 6$ ($S = 5/2$). When the cluster is doped by Rh, the ground state is a non-magnetic, $S = 0$. Thus, the lowest energy for a magnetic state for the cluster doped by Rh corresponds to $M = 3$ ($S = 1$). In the case of Pd, the ground state has $M = 4$ ($S = 3/2$). The values of the operator S^2 after correction on the spin contamination practically agree with the correct

value $S(S+1)$, except when $S = 1/2$. This indicates that all calculated energies with only one mentioned exception can be accepted as correct.

3.2. Natural Bond Orbital Analysis

In Table 2 and Table 3, the atomic charge and the valence orbital population at the NBO level for the central and nearest neighbors (n.n.) atoms are presented. The outer atoms of As and Ba are not presented because they are on the boundary of the cluster. Although the excited Rydberg orbitals are not presented, they are taken into account for calculating the atomic charges.

According to Table 2, the central atom of the pure cluster is almost neutral for the embedded cluster, whereas it is almost one electron for the isolated cluster. After doping by Rh and Pd, a large negative charge appears on both dopant atoms, for the isolated and embedded cluster. For As(n.n.), a decrease in the negative charge is observed, it is associated with the charge transfer from As(n.n.) to the dopant atom. Whereas, in all Fe(n.n.) a small change in their charge is observed. Thus, there is a charge transfer from As(n.n.) atoms to dopants. This situation is the same for isolated and embedded cluster.

Table 1. Energy of the states calculated at the MP2 level using GAUSSIAN 2016 A.03 according to different multiplicities for the embedded and isolated cluster, pure and doped.

Multiplicity	Embedded Cluster		Isolated Cluster	
$Ba_4Fe_5As_8$	Energy (a.u.)	S^2 ($\hbar^2$)	Energy (a.u.)	S^2 ($\hbar^2$)
2	−24,310.14749	0.75 (0.75)	−24,292.584548	0.75 (0.75)
4	−24,310.14388	3.75 (3.75)	−24,292.564423	3.75 (3.77)
6	−24,310.20111	8.75 (8.75)	−24,292.618489	8.75 (8.82)
8	−24,310.10686	15.75 (15.75)	−24,292.715159	15.75 (15.76)
10			−24,292.675436	24.75 (24.76)
$Ba_4Fe_4RhAs_8$				
1	−24,141.44594	0 (0.00)	−23,140.426635	0 (0)
3	−24,141.42368	2 (2.00)	−23,139.851233	2 (2.00)
5	−24,141.30910	6 (6.06)	−23,139.941032	6 (6.08)
7	−24,141.27509	12 (12.01)	−23,139.917454	12 (12.06)
$Ba_4Fe_4PdAs_8$				
2	−23,174.63554	0.75 (2.93)	−23,157.175340	0.75 (1.07)
4	−23,174.61090	3.75 (3.76)	−23,157.088309	3.75 (12.13)
6	−23,174.58909	8.75 (8.76)	−23,157.208473	8.75 (8.77)
8	−23,174.52517	15.75 (15.76)	−23,157.117429	15.75 (15.87)

Table 2. NBO charge distribution at the ground state of the embedded and isolated cluster, pure and doped, at the MP2 level.

	Embedded Cluster		**Isolated Cluster**	
	Atomic Charge	Valence orbital population	Atomic Charge	Valence orbital population
$Ba_4Fe_5As_8$	$S=5/2$		$7/2$	
Fe	0.08	$4s^{0.4}3d^{7.45}$	0.73	$4s^{0.45}3d^{6.65}$
Fe (n.n.)a	0.76	$4s^{0.47}3d^{6.64}$	0.78	$4s^{0.50}3d^{6.57}$
Fe (n.n.)b	0.49	$4s^{1.03}3d^{6.36}$	0.73	$4s^{0.78}3d^{6.39}$
As (n.n.)	−1.49	$4s^{1.82}4p^{4.53}$	−1.50	$4s^{1.81}4p^{4.51}$
$Ba_4Fe_4RhAs_8$	$S=1$		$S=2$	
Rh	−2.61	$5s^{0.55}4d^{9.10}5p^{1.72}$	−2.77	$5s^{0.50}4d^{9.00}5p^{2.03}$
Fe (n.n.)a	0.68	$4s^{0.45}3d^{6.74}$	0.83	$4s^{0.55}3d^{6.49}$
Fe (n.n.)b	0.18	$4s^{1.38}3d^{6.32}$	0.77	$4s^{0.81}3d^{6.44}$
As (n.n.)	−0.64	$4s^{1.68}4p^{3.83}$	−0.79	$4s^{1.65}4p^{4.02}$
$Ba_4Fe_4PdAs_8$	$S=3/2$		$S=5/2$	
Pd	−1.74	$5s^{0.46}4d^{9.20}5p^{1.85}$	−2.17	$5s^{0.49}4d^{9.29}5p^{2.12}$
Fe (n.n.)a	0.84	$4s^{0.45}3d^{6.59}$	0.58	$4s^{0.42}3d^{6.88}$
Fe (n.n.)b	0.24	$4s^{0.98}3d^{6.70}$	0.81	$4s^{0.81}3d^{6.30}$
As (n.n.)	−0.9	$4s^{1.65}4p^{4.10}$	−0.94	$4s^{1.65}4p^{4.15}$

Table 3. NBO detailed valence orbital population at the ground state of the embedded and isolated cluster, pure and doped, at the MP2 level.

	Embedded Cluster	**Isolated Cluster**
	Detailed charge orbital population for $3d$ (Fe), $4d$ (Rh, Pd), $5p$ (Rh, Pd) and $4p$ (As)	Detailed charge orbital population for $3d$ (Fe), $4d$ (Rh, Pd), $5p$ (Rh, Pd) and $4p$ (As)
$Ba_4Fe_5As_8$	$S=5/2$	$S=7/2$
Fe	$d_{xy}^{1.72}+d_{xz}^{0.66}+d_{yz}^{1.14}+d_{x^2-y^2}^{1.96}+d_{z^2}^{1.96}$	$d_{xy}^{1.92}+d_{xz}^{1.91}+d_{yz}^{0.59}+d_{x^2-y^2}^{0.65}+d_{z^2}^{1.58}$
Fe (n.n.)a	$d_{xy}^{1.28}+d_{xz}^{1.09}+d_{yz}^{0.64}+d_{x^2-y^2}^{1.81}+d_{z^2}^{1.82}$	$d_{xy}^{1.18}+d_{xz}^{1.03}+d_{yz}^{0.80}+d_{x^2-y^2}^{1.64}+d_{z^2}^{1.91}$
Fe (n.n.)b	$d_{xy}^{0.65}+d_{xz}^{0.88}+d_{yz}^{1.45}+d_{x^2-y^2}^{1.78}+d_{z^2}^{1.55}$	$d_{xy}^{1.60}+d_{xz}^{1.75}+d_{yz}^{0.66}+d_{x^2-y^2}^{0.92}+d_{z^2}^{1.44}$
As (n.n.)	$p_x^{1.52}+p_y^{1.57}+p_z^{1.44}$	$p_x^{1.44}+p_y^{1.56}+p_z^{1.50}$
$Ba_4Fe_4RhAs_8$	$S=1$	$S=2$
Rh	$d_{xy}^{1.56}+d_{xz}^{1.81}+d_{yz}^{2.17}+d_{x^2-y^2}^{1.93}+d_{z^2}^{1.63}$ $p_x^{0.51}+p_y^{0.61}+p_z^{0.61}$	$d_{xy}^{1.79}+d_{xz}^{1.90}+d_{yz}^{1.56}+d_{x^2-y^2}^{1.94}+d_{z^2}^{1.80}$ $p_x^{0.60}+p_y^{0.72}+p_z^{0.70}$
Fe (n.n.)a	$d_{xy}^{1.74}+d_{xz}^{0.69}+d_{yz}^{0.77}+d_{x^2-y^2}^{1.73}+d_{z^2}^{1.81}$	$d_{xy}^{1.45}+d_{xz}^{0.74}+d_{yz}^{0.72}+d_{x^2-y^2}^{1.65}+d_{z^2}^{1.94}$
Fe (n.n.)b	$d_{xy}^{1.52}+d_{xz}^{1.78}+d_{yz}^{0.6}+d_{x^2-y^2}^{1.05}+d_{z^2}^{1.48}$	$d_{xy}^{1.80}+d_{xz}^{1.95}+d_{yz}^{1.95}+d_{x^2-y^2}^{0.25}+d_{z^2}^{0.39}$
As (n.n.)	$p_x^{1.11}+p_y^{1.49}+p_z^{1.23}$	$p_x^{1.28}+p_y^{1.28}+p_z^{1.46}$
$Ba_4Fe_4PdAs_8$	$S=3/2$	$S=5/2$
Pd	$d_{xy}^{1.89}+d_{xz}^{1.69}+d_{yz}^{1.74}+d_{x^2-y^2}^{1.96}+d_{z^2}^{1.91}$ $p_x^{0.58}+p_y^{0.6}+p_z^{0.67}$	$d_{xy}^{1.87}+d_{xz}^{1.83}+d_{yz}^{1.74}+d_{x^2-y^2}^{1.96}+d_{z^2}^{1.88}$ $p_x^{0.65}+p_y^{0.74}+p_z^{0.73}$
Fe (n.n.)a	$d_{xy}^{1.9}+d_{xz}^{0.48}+d_{yz}^{1.02}+d_{x^2-y^2}^{1.36}+d_{z^2}^{1.82}$	$d_{xy}^{1.63}+d_{xz}^{0.83}+d_{yz}^{0.68}+d_{x^2-y^2}^{1.82}+d_{z^2}^{1.91}$
Fe (n.n.)b	$d_{xy}^{0.56}+d_{xz}^{1.92}+d_{yz}^{1.91}+d_{x^2-y^2}^{1.96}+d_{z^2}^{0.35}$	$d_{xy}^{1.78}+d_{xz}^{1.95}+d_{yz}^{1.95}+d_{x^2-y^2}^{0.27}+d_{z^2}^{0.34}$
As (n.n.)	$p_x^{1.24}+p_y^{1.39}+p_z^{1.47}$	$p_x^{1.42}+p_y^{1.37}+p_z^{1.36}$

It is instructive to compare the obtained valence orbital population for the embedded and isolated pure cluster with the valence orbital population of free atoms: Fe: [Ar] $3d^6 4s^2$ and As: [Ar] $4s^2 4p^3$. According to Table 2, for the embedded pure cluster, the Fe atoms in the pure cluster show a decrease in its 4s orbital population of 1.6e for the central atom, 1.53e for the Fe(n.n.)a, and 0.97e for the Fe(n.n.)b. The population of the 3d orbitals is increased by 1.45e on the central atom, 0.64e on the Fe(n.n.)a, and 0.36e on the Fe(n.n.)b. On As(n.n.) a decrease is observed in the 4s orbital population of 0.51e and an increase of 1.53e on the orbital 4p. On the other hand, for the isolated pure cluster, there is also a decrease on the 4s orbital by 1.55e for the central Fe, by 1.5e for the Fe(n.n.)a, and by 1.22e for the Fe(n.n.)b; a and b denote the crystallographic directions. The 3d orbital population increased by 0.65e for the central atom, by 0.57e for the Fe(n.n.)a, and by 0.39e for the Fe(n.n.)b. On As(n.n.) a decrease by 0.19e on the orbital 4s and an increase by 1.51e on the orbital 4p are observed.

Let us return to Table 2 and Table 3. In comparison with the population of free atoms (Rh: [Kr] $4d^8 5s^1$ and Pd: [Kr] $4d^{10}$, as follows from Table 2, for the isolated and embedded cluster for both doping, it is observed the charge transfers from As(n.n.) atoms to the dopant atoms, that can be due to the screening effect. As follows from Table 3 for both doping, the 3d orbital population on Fe(n.n.) depends on direction of the orbitals.

In Table 4 and Table 5, the spin orbital population at the NBO level for the ground state of embedded and isolated cluster, pure and doped, are presented. As follows from Table 4 for the embedded pure cluster, the spin on the central Fe is equal to 0.32 $\hbar$, whereas for the isolated cluster, the spin on the central Fe atom is almost cero. For the embedded cluster the spin is practically absent on both dopant atoms, whereas for the isolated cluster the Rh dopant has $S = -0.51$ $\hbar$. In the case of the isolated cluster, all atoms are practically spinless except As(n.n.) for Rh doping and Fe(n.n.)a for Pd doping. For embedded doped clusters, the distribution of the spin orbital population does not change comparing with the pure clusters. In the case of the isolated cluster for Rh doping, the β-electrons transfer to the Rh atom, whereas α-electron transfers to As(n.n.). For Pd doping, the β-electrons transfer to Fe(n.n.)a.

As follows from Table 5 for the detailed spin valence orbital population, for the Rh doping there is a β-spin density population on d_{xy} and d_{yz}, whereas for Pd doping there is the zero-spin density on all orbitals. We would like to mention that for Pd doping, the spin density population does not depend on direction of Fe(n.n.). Also, for Rh doping there is spin density population for the Fe(n.n.)a on the d_{xy} and d_{xz} where α and β-spin density populations are observed.

The spin distribution obtained in Table 5 is in agreement with the charge distribution in Table 3. We would like to mention that for the embedded cluster in the case of Rh doping, the orbitals d_{xz} and d_{yz} of Fe(n.n.)a, and d_{yz} and $d_{x^2-y^2}$ of Fe(n.n.)b are practically occupied by one electron with zero spin population. For the Pd doping, on the orbital d_{yz} of Fe(n.n.)a there is also one electron with zero

spin population. The spinless electron resembles the spinless holons proposed by Anderson in his RVB model of high T_c-SC [55] [56].

Table 4. NBO spin distribution at the ground state of the embedded and isolated cluster, pure and doped, at the MP2 level.

	Embedded Cluster		Isolated Cluster	
	Spin ($\hbar$)	Valence orbital spin population	Spin ($\hbar$)	Valence orbital spin population
$Ba_4Fe_5As_8$		$S=5/2$		$S=7/2$
Fe	0.32	$4s^{-0.01}3d^{0.33}$	−0.03	$4s^{0}3d^{-0.04}$
Fe (n.n.)a	0.07	$4s^{0.01}3d^{0.06}$	0.08	$4s^{-0.02}3d^{0.08}$
Fe (n.n.)b	0.65	$4s^{0.59}3d^{0.06}$	−0.01	$4s^{0}3d^{-0.03}$
As (n.n.)	0.23	$4s^{0.02}4p^{0.21}$	−0.02	$4s^{0.01}4p^{-0.04}$
$Ba_4Fe_4RhAs_8$		$S=1$		$S=2$
Rh	−0.05	$5s^{0}4d^{-0.05}5p^{0}$	−0.51	$5s^{0}4d^{-0.84}5p^{0.29}$
Fe (n.n.)a	0.03	$4s^{0.01}3d^{0.02}$	0.06	$4s^{0.11}3d^{-0.03}$
Fe (n.n.)b	0.04	$4s^{-0.02}3d^{0.02}$	0.09	$4s^{0.02}3d^{-0.02}$
As (n.n.)	0.02	$4s^{0}4p^{0.02}$	0.33	$4s^{0}4p^{-0.31}$
$Ba_4Fe_4PdAs_8$		$S=3/2$		$S=5/2$
Pd	−0.04	$5s^{0.02}4d^{-0.08}5p^{0.02}$	0.07	$5s^{0.01}4d^{0.04}5p^{0.03}$
Fe (n.n.)a	−0.01	$4s^{0.01}3d^{-0.02}$	−0.37	$4s^{-0.02}3d^{-0.34}$
Fe (n.n.)b	0.96	$4s^{0.33}3d^{0.63}$	0.05	$4s^{0}3d^{0.02}$
As (n.n.)	0	$4s^{0}4p^{0}$	−0.07	$4s^{0.01}4p^{-0.05}$

Table 5. NBO detailed spin valence orbital population at the ground state of the embedded and isolated cluster, pure and doped, at the MP2 level.

	Embedded Cluster	Isolated Cluster
	Detailed spin orbital population for $3d$ (Fe), $4d$ (Rh, Pd), $5p$ (Rh, Pd) and $4p$ (As)	Detailed spin orbital population for $3d$ (Fe), $4d$ (Rh, Pd), $5p$ (Rh, Pd) and $4p$ (As)
$Ba_4Fe_5As_8$	$S=5/2$	$S=7/2$
Fe	$d_{xy}^{-0.62}+d_{xz}^{0.12}+d_{yz}^{0.82}+d_{x^2-y^2}^{0}+d_{z^2}^{0.01}$	$d_{xy}^{-0.01}+d_{xz}^{-0.01}+d_{yz}^{-0.01}+d_{x^2-y^2}^{0.01}+d_{z^2}^{-0.02}$
Fe (n.n.)a	$d_{xy}^{0.1}+d_{xz}^{-0.07}+d_{yz}^{0.02}+d_{x^2-y^2}^{0.01}+d_{z^2}^{0}$	$d_{xy}^{-0.01}+d_{xz}^{0.13}+d_{yz}^{-0.05}+d_{x^2-y^2}^{-0.03}+d_{z^2}^{0.04}$
Fe (n.n.)b	$d_{xy}^{0.18}+d_{xz}^{0.06}+d_{yz}^{-0.07}+d_{x^2-y^2}^{0}+d_{z^2}^{-0.11}$	$d_{xy}^{-0.03}+d_{xz}^{00.2}+d_{yz}^{0}+d_{x^2-y^2}^{-0.01}+d_{z^2}^{-0.01}$
As (n.n.)	$p_x^{0.07}+p_y^{0}+p_z^{0.14}$	$p_x^{-0.04}+p_y^{-0.04}+p_z^{0}$
$Ba_4Fe_4RhAs_8$	$S=1$	$S=2$
Rh	$d_{xy}^{-0.01}+d_{xz}^{0.01}+d_{yz}^{-0.06}+d_{x^2-y^2}^{0}+d_{z^2}^{0.01}$ $p_x^{0}+p_y^{0}+p_z^{0}$	$d_{xy}^{-0.01}+d_{xz}^{-0.36}+d_{yz}^{-0.46}+d_{x^2-y^2}^{0}+d_{z^2}^{-0.01}$ $p_x^{0.04}+p_y^{0.25}+p_z^{0}$
Fe (n.n.)a	$d_{xy}^{0}+d_{xz}^{0.01}+d_{yz}^{0.04}+d_{x^2-y^2}^{-0.02}+d_{z^2}^{-0.01}$	$d_{xy}^{0.38}+d_{xz}^{-0.38}+d_{yz}^{0.01}+d_{x^2-y^2}^{-0.09}+d_{z^2}^{0.05}$
Fe (n.n.)b	$d_{xy}^{-0.02}+d_{xz}^{0}+d_{yz}^{0.01}+d_{x^2-y^2}^{0.03}+d_{z^2}^{0}$	$d_{xy}^{0.01}+d_{xz}^{0.01}+d_{yz}^{-0.01}+d_{x^2-y^2}^{-0.03}+d_{z^2}^{0}$
As (n.n.)	$p_x^{0.01}+p_y^{0.01}+p_z^{0}$	$p_x^{0.11}+p_y^{-0.21}+p_z^{-0.21}$
$Ba_4Fe_4PdAs_8$	$S=3/2$	$S=5/2$
Pd	$d_{xy}^{-0.01}+d_{xz}^{-0.04}+d_{yz}^{-0.02}+d_{x^2-y^2}^{0}+d_{z^2}^{-0.01}$ $p_x^{0.01}+p_y^{0}+p_z^{0.03}$	$d_{xy}^{-0.01}+d_{xz}^{0.05}+d_{yz}^{0}+d_{x^2-y^2}^{0}+d_{z^2}^{0}$ $p_x^{-0.05}+p_y^{0.08}+p_z^{0}$
Fe (n.n.)a	$d_{xy}^{-0.02}+d_{xz}^{0.01}+d_{yz}^{-0.03}+d_{x^2-y^2}^{0.02}+d_{z^2}^{0}$	$d_{xy}^{-0.07}+d_{xz}^{-0.15}+d_{yz}^{-0.16}+d_{x^2-y^2}^{0.03}+d_{z^2}^{0.01}$
Fe (n.n.)b	$d_{xy}^{0.47}+d_{xz}^{0.01}+d_{yz}^{0.01}+d_{x^2-y^2}^{-0.01}+d_{z^2}^{0.15}$	$d_{xy}^{0}+d_{xz}^{0.01}+d_{yz}^{0.01}+d_{x^2-y^2}^{0}+d_{z^2}^{0}$
As (n.n.)	$p_x^{0}+p_y^{0}+p_z^{0}$	$p_x^{-0.01}+p_y^{-0.02}+p_z^{-0.02}$

4. Conclusions

As follows from the discussion of our calculations by unrestricted open shell ECM-MP2, the ground state for the isolated cluster is characterized by a different multiplicity than the ground state of the embedded cluster. The background charges modify the energy of the cluster and the valence orbital population. It is also revealed that the calculation by unrestricted open shell MP2 method leads in some cases to high spin contamination of the state.

For the isolated cluster doped by Rh and Pd, we obtained a decrease in population of some valence orbitals. The orbital population for Fe(n.n.) depends on direction, this is in agreement with experiments. For the doped isolated cluster, a charge transfer from the As(n.n.) atoms to the central atom was observed, as in the case of the embedded cluster. Thus, for the embedded and isolated clusters for Rh and Pd doping, the charge transfers from nearest neighbor atoms to the dopants, whereas only for the isolated cluster doped by Rh we obtained spin transfer.

It is important to mention that for both dopants, the spin disappears on the dopants and the charge and spin transfer are completely independent. Thus, obtained in our calculations charge and spin orbital distributions, are in agreement with the spinless electrons proposed by Anderson (Anderson's holon). This indicates the possibility of the superconductivity mechanism in this material proposed by Anderson in his RVB theory.

Acknowledgements

The authors thank the DGTIC computer staff for providing access to the MITZLI cluster of Universidad Nacional Autónoma de México. This work was partly supported by grants from DGAPA PAPIT IN111519. We also gratitude Lic. Alejandro Pompa-García and Tec. Cain González for their technical support.

Conflicts of Interest

The authors declare no conflicts of interest regarding the publication of this paper.

References

[1] Kamerling Onnes, H. (1911) On the Change in the Resistance of Pure Metals at Very Low Temperatures. III The Resistance of Platinum at Helium Temperatures. *Communications*, *Leiden*, **124c**, 799-802.

[2] Heisenberg, W. (1925) Quantum-Theoretical Re-Interpretation of Kinematic and Mechanical Relations. *Zeitschrift für Physik*, **33**, 879-893. https://doi.org/10.1007/BF01328377

[3] Born, M. and Jordan, P. (1925) Zur Quantenmechanik. *Zeitschrift für Physik*, **34**, 858-888. https://doi.org/10.1007/BF01328531

[4] de Broglie, L. (1925) Recherches sur la Théorie des Quanta. *Annals of Physics*, **3**, 122-128. https://doi.org/10.1051/anphys/192510030022

[5] Schrödinger, E. (1926) On the Relation between the Quantum Mechanics of Heisenberg, Born, and Jordan, and That of Schrödinger. *Annals of Physics*, **79**, 361-376, 489-527, 734-756. https://doi.org/10.1002/andp.19263840804

[6] Schrödinger, E. (1926) An Undulatory Theory of the Mechanics of Atoms and Molecules. *Physical Review*, **28**, 1049-1070. https://doi.org/10.1103/PhysRev.28.1049

[7] Pauli, W. (1925) Über den Zusammenhang des Abschlusses der Elektronengruppen im Atom mit der Komplexstruktur der Spektren. *Zeitschrift für Physik*, **31**, 765-783. https://doi.org/10.1007/BF02980631

[8] Dirac, P.A.M. (1926) On the Theory of Quantum Mechanics. *Proceedings of the Royal Society of London. Series A*, **112**, 661-677. https://doi.org/10.1098/rspa.1926.0133

[9] Dirac, P.A.M. (1927) The Quantum Theory of the Emission and Absorption of Radiation. *Proceedings of the Royal Society of London. Series A*, **114**, 243-265. https://doi.org/10.1098/rspa.1927.0039

[10] Bardeen, J., Cooper, L.N. and Schrieffer, J.R. (1957) Microscopic Theory of Superconductivity. *Physical Review*, **106**, 162-164. https://doi.org/10.1103/PhysRev.106.162

[11] Bardeen, J., Cooper, L.N. and Schrieffer, J.R. (1957) Theory of Superconductivity. *Physical Review*, **108**, 1175-1204. https://doi.org/10.1103/PhysRev.108.1175

[12] Gor'kov, L.P. (1959) Microscopic Derivation of the Ginzburg-Landau Equations in the Theory of Superconductivity. *Soviet Physics JETP*, **36**, 1364-1367.

[13] Ginzburg, V.L. and Landau, L.D. (1950) On the Theory of Superconductivity. *Soviet Physics JETP*, **20**, 1064.

[14] Ginzburg, L.D. and Landau L.D. (2009) On the Theory of Superconductivity. In: *On Superconductivity and Superfluidity*, Springer, Berlin, 113-137.

[15] Éliashberg, G.M. (1960) Interactions between Electrons and Lattice Vibrations in a Superconductor. *Soviet Physics JETP*, **11**, 696-702.

[16] Bednorz, J.G. and Müller, K.A. (1986) Possible High T*c* Superconductivity in the Ba-La-Cu-O System. *Zeitschrift für Physik B—Condensed Matter*, **64**, 189-193. https://doi.org/10.1007/BF01303701

[17] Bucher, B., Karpinski, J., Kaldis, E. and Wachter, P. (1989) Strong Pressure Dependence of Tc of the New 80 K Phase $YBa_2Cu_4O_{8+x}$. *Physica C*: *Superconductivity*, **157**, 478. https://doi.org/10.1016/0921-4534(89)90273-6

[18] Hor, P.H., Gao, L., Meng, R.L., Huang, Z.J., *et al.* (1987) High-Pressure Study of the New Y-Ba-Cu-O Superconducting Compound System. *Physical Review Letters*, **58**, 911. https://doi.org/10.1103/PhysRevLett.58.911

[19] Han, S.H., *et al.* (1988) Pressure Effects on the New High-Tc Superconductor Tl-Ba-Ca-Cu-O. *Physica C*: *Superconductivity*, **156**, 113-115. https://doi.org/10.1016/0921-4534(88)90114-1

[20] Maple, M.B., Ayoub, N.Y., Bjørnholm, T., Early, E.A., *et al.* (1989) Magnetism, Specific Heat, and Pressure-Dependent Resistivity of the Electron-Doped Compounds $Ln_{2-x}M_xCuO_{4-y}$ (Ln = Pr, Nd, Sm, Eu, Gd; M = Ce, Th). *Physica C*: *Superconductivity and Its Applications*, **162**-**164**, 296. https://doi.org/10.1016/0921-4534(89)91029-0

[21] Drozdov, A.P., Eremets, M.I., Troyan, I.A., Ksenofontov, V. and Shylin, S.I. (2015) Conventional Superconductivity at 203 K at High Pressures in the Sulfur Hydride System. *Nature*, **525**, 73-76. https://doi.org/10.1038/nature14964

[22] Snider, E., Dasenbrock-Gammon, N., McBride, R., Debessai, M., *et al.* (2020)

Room-Temperature Superconductivity in a Carbonaceous Sulfur Hydride. *Nature*, **586**, 373-377. https://doi.org/10.1038/s41586-020-2801-z

[23] Kamihara, Y., Watanabe, M. and Hosono, H. (2008) Iron-Based Layered Superconductor La[$O_{1-x}F_x$]FeAs (x = 0.05−0.12) with Tc = 26 K. *Journal of the American Chemical Society*, **130**, 3296-3297. https://doi.org/10.1021/ja800073m

[24] Takahashi, H., Igawa, K., Arii, K., Kamihara, Y., Hirano, M. and Hosono, H. (2008) Superconductivity at 43 K in an Iron-Based Layered Compound $LaO_{1-x}F_xFeAs$. *Nature* (*London*), **453**, 376-378. https://doi.org/10.1038/nature06972

[25] Stewart, R.G. (2011) Superconductivity in Iron Compounds. *Reviews of Modern Physics*, **83**, 1589. https://doi.org/10.1103/RevModPhys.83.1589

[26] Rotter, M., Tegel, M. and Johrendt, D. (2008) Superconductivity at 38 K in the Iron Arsenide $(Ba_{1-x}K_x)Fe_2As_2$. *Physical Review Letters*, **101**, Article ID: 107006. https://doi.org/10.1103/PhysRevLett.101.107006

[27] Sefat, A.S., Jin, R., McGuire, M.A., Sales, B.C., Singh, D.J. and Mandrus, D. (2008) Superconductivity at 22 K in Co-Doped $BaFe_2As_2$ Crystals. *Physical Review Letters*, **101**, Article ID: 117004. https://doi.org/10.1103/PhysRevLett.101.117004

[28] Ni, N., Tillman, M.E., Yan, J.-Q., Kracher, A., Hannahs, S.T., Bud'ko, S.L. and Canfield, P.C. (2008) Effects of Co Substitution on Thermodynamic and Transport Properties and Anisotropic Hc2 in $Ba(Fe_{1-x}Co_x)_2As_2$ Single Crystals. *Physical Review B*, **78**, Article ID: 214515. https://doi.org/10.1103/PhysRevB.78.214515

[29] Kondo, T., Fernandes, R.M., Khasanov, R., Liu, Ch., Palczewski, A.D., *et al.* (2010) Rapid Communication Unexpected Fermi-Surface Nesting in the Pnictide Parent Compounds $BaFe_2As_2$ and $CaFe_2As_2$ Revealed by Angle-Resolved Photoemission Spectroscopy. *Physical Review B*, **81**, Article ID: 060507. https://doi.org/10.1103/PhysRevB.81.060507

[30] Canfield, P.C., Bud'ko, S.L., Ni, N., Yan, J.Q. and Kracher, A. (2009) Decoupling of the Superconducting and Magnetic/Structural Phase Transitions in Electron-Doped $BaFe_2As_2$. *Physical Review B*, **80**, Article ID: 060501. https://doi.org/10.1103/PhysRevB.80.060501

[31] Mun, E.D., Bud'ko, S.L., Ni, N., Thaler, A.N. and Canfield, P.C. (2009) Thermoelectric Power and Hall Coefficient Measurements on $Ba(Fe_{1-x}T_x)_2As_2$ (T = Co and Cu). *Physical Review* B, **80**, Article ID: 054517. https://doi.org/10.1103/PhysRevB.80.054517

[32] Ni, N., Thaler, A., Kracher, A., Yan, J.Q., Bud'ko, S.L. and Canfield, P.C. (2009) Phase Diagrams of $Ba(Fe_{1-x}M_x)_2As_2$ Single Crystals (M = Rh and Pd). *Physical Review B*, **80**, Article ID: 024511. https://doi.org/10.1103/PhysRevB.80.024511

[33] Mazin, I.I., Singh, D.J., Johannes, M.D. and Du, M.H. (2008) Unconventional Superconductivity with a Sign Reversal in the Order Parameter of $LaFeAsO_{1-x}F_x$. *Physical Review Letters*, **101**, Article ID: 057003. https://doi.org/10.1103/PhysRevLett.101.057003

[34] Mazin, I.I. and Schmalian, J. (2009) Pairing Symmetry and Pairing State in Ferropnictides: Theoretical Overview. *Physica C*: *Superconductivity*, **469**, 614-627. https://doi.org/10.1016/j.physc.2009.03.019

[35] Singh, D.J. and Du, M.H. (2008) Density Functional Study of $LaFeAsO_{1-x}F_x$: A Low Carrier Density Superconductor near Itinerant Magnetism. *Physical Review Letters*, **100**, Article ID: 237003. https://doi.org/10.1103/PhysRevLett.100.237003

[36] Norman, M.R. (2008) High-Temperature Superconductivity in the Iron Pnictides. *Physics*, **1**, 21. https://doi.org/10.1103/Physics.1.21

[37] Norman, M.R. (2011) The Challenge of Unconventional Superconductivity. *Science*, **332**, 196-200. https://doi.org/10.1126/science.1200181

[38] Mazin, I.I. (2010) Superconductivity Gets an Iron Boost. *Nature*, **464**, 183-186. https://doi.org/10.1038/nature08914

[39] Wang, F. and Lee, D.H. (2011) The Electron-Pairing Mechanism of Iron-Based Superconductors. *Science*, **332**, 200. https://doi.org/10.1126/science.1200182

[40] Chubukov, A. (2012) Pairing Mechanism in Fe-Based Superconductors. *Annual Review of Condensed Matter Physics*, **3**, 57-92. https://doi.org/10.1146/annurev-conmatphys-020911-125055

[41] Kordyuk, A.A. (2012) Iron-Based Superconductors: Magnetism, Superconductivity, and Electronic Structure (Review Article). *Low Temperature Physics*, **38**, 888. https://doi.org/10.1063/1.4752092

[42] Baquero, R. (2014) La Superconductividad: Sus orígenes, sus teorías, sus problemas candentes hoy. *Revista de la Academia Colombiana de Ciencias*, **38**, 18-33. https://doi.org/10.18257/raccefyn.152

[43] Prozorov, R., Kończykowski, M., Tanatar, M.A., Wen, H.H., Fernandes, R.M. and Canfield, P.C. (2019) Interplay between Superconductivity and Itinerant Magnetism in Underdoped $Ba_{1-x}K_xFe_2As_2$ (x = 0.2) Probed by the Response to Controlled Point-Like Disorder. *NPJ Quantum Materials*, **4**, Article No. 34. https://doi.org/10.1038/s41535-019-0171-2

[44] Kuroki, K., Onari, S., Arita, R., Usui, H., Tanaka, Y., Kontani, H. and Aoki, H. (2008) Unconventional Pairing Originating from the Disconnected Fermi Surfaces of Superconducting $LaFeAsO_{1-x}F_x$. *Physical Review Letters*, **101**, Article ID: 087004. https://doi.org/10.1103/PhysRevLett.101.087004

[45] Takimoto, T., Hotta, T. and Ueda, K. (2004) Strong-Coupling Theory of Superconductivity in a Degenerate Hubbard Model. *Physical Review B*, **69**, Article ID: 104504. https://doi.org/10.1103/PhysRevB.69.104504

[46] Onari, S. and Kontani, H. (2009) Violation of Anderson's Theorem for the Sign-Reversing s-Wave State of Iron-Pnictide Superconductors. *Physical Review Letters*, **103**, Article ID: 177001. https://doi.org/10.1103/PhysRevLett.103.177001

[47] Kontani, H. and Onari, S. (2010) Orbital-Fluctuation-Mediated Superconductivity in Iron Pnictides: Analysis of the Five-Orbital Hubbard-Holstein Model. *Physical Review Letters*, **104**, Article ID: 157001. https://doi.org/10.1103/PhysRevLett.104.157001

[48] Si Q. and Abrahams, E. (2008) Strong Correlations and Magnetic Frustration in the High Tc Iron Pnictides. *Physical Review Letters*, **101**, Article ID: 076401. https://doi.org/10.1103/PhysRevLett.101.076401

[49] Chen, W.Q., Yang, K.Y., Zhou, Y. and Hang, F.C., (2009) Strong Coupling Theory for Superconducting Iron Pnictides. *Physical Review Letters*, **102**, Article ID: 047006. https://doi.org/10.1103/PhysRevLett.102.047006

[50] Qazilbash, M.M., Hamlin, J.J., Baumbach, R.E., Zhang, L., Singh, D.J., Maple, M.B. and Basov, D.N. (2009) Electronic Correlations in the Iron Pnictides. *Nature Physics*, **5**, 647-650. https://doi.org/10.1038/nphys1343

[51] Haule, K., Shim, J.H. and Kotliar, G. (2008) Correlated Electronic Structure of $LaO_{1-x}F_xFeAs$. *Physical Review Letters*, **100**, Article ID: 226402. https://doi.org/10.1103/PhysRevLett.100.226402

[52] Laad, M.S., Craco, L., Leoni, S. and Rosner, H (2009) Electrodynamic Response of Incoherent Metals: Normal Phase of Iron Pnictides. *Physical Review B*, **79**, Article ID: 024515. https://doi.org/10.1103/PhysRevB.79.024515

[53] Lee, P.A., Nagaosa, N. and Wen, X.G. (2006) Doping a Mott Insulator: Physics of High-Temperature Superconductivity. *Reviews of Modern Physics*, **78**, 17. https://doi.org/10.1103/RevModPhys.78.17

[54] Anderson, P.W. (1987) The Resonating Valence Bond State in La_2CuO_4 and Superconductivity. *Science*, **235**, 1196-1198. https://doi.org/10.1126/science.235.4793.1196

[55] Kivelson, S.A., Rokhsar, D.S. and Sethna, J.P. (1987) Topology of the Resonating Valence-Bond State: Solitons and High-Tc Superconductivity. *Physical Review B*, **35**, 8865. https://doi.org/10.1103/PhysRevB.35.8865

[56] Anderson, P.W., Baskaran, G., Zou, Z. and Hsu, T. (1987) Resonating-Valence-Bond Theory of Phase Transitions and Superconductivity in La_2CuO_4-Based Compounds. *Physical Review Letters*, **58**, 2790. https://doi.org/10.1103/PhysRevLett.58.2790

[57] Soullard, J., Pérez-Enriquez, R. and Kaplan, I. (2015) Comparative Study of Pure and Co-Doped $BaFe_2As_2$. *Physical Review B*, **91**, Article ID: 184517. https://doi.org/10.1103/PhysRevB.91.184517

[58] Soullard, J. and Kaplan, I. (2016) Comparative Study of the Magnetic Structure of $BaFe_2As_2$ Doped with Co or Ni. *Journal of Superconductivity and Novel Magnetism*, **29**, 3147-3154. https://doi.org/10.1007/s10948-016-3626-8

[59] Columbié-Leyva, R., Soullard, J. and Kaplan, I. (2019) Electronic Structure Study of New Family of High-Tc Fe-Superconductors Based on $BaFe_2As_2$ in Presence of Dopants Rh and Pd. *MRS Advances*, **4**, 3365-3372. https://doi.org/10.1557/adv.2019.409

[60] Kaplan, I.G., Soullard, J., Hernández-Cobos, J. and Pandey, R. (1999) Electronic Structure of Ceramics at the MP2 Electron Correlation Level. *Journal of Physics: Condensed Matter*, **11**, 1049-1058. https://doi.org/10.1088/0953-8984/11/4/012

[61] Kaplan, I.G., Hernández-Cobos, J. and Soullard, J. (2000) Quantum Systems in Chemistry and Physics. Kluwer Academic, Dordrecht, 143-158.

[62] Kaplan, I.G., Soullard, J. and Hernández-Cobos, J. (2002) Effect of Zn and Ni Substitution on the Local Electronic Structure of the $YBa_2Cu_3O_7$ Superconductor. *Physical Review B*, **65**, Article ID: 214509. https://doi.org/10.1103/PhysRevB.65.214509

[63] Foster, J.P. and Weinhold, F. (1980) Natural Hybrid Orbitals. *Journal of the American Chemical Society*, **102**, 7211-7218. https://doi.org/10.1021/ja00544a007

[64] Weinhold, F. and Landis, C.R. (2001) Natural Bond Orbitals and Extensions of Localized Bonding Concepts. *Chemistry Education Research and Practice*, **2**, 91-104. https://doi.org/10.1039/B1RP90011K

[65] Glendening, E.D., Reed, A.E., Carpenter, J.E. and Weinhold, F. (2003) NBO Version 3.1.

[66] Frisch, M.J., Trucks, G.W., *et al.* (2016) Gaussian 16 Revision A.03.

[67] Kaplan, I.G. (2006) Intermolecular Interaction: Physical Picture, Computational Methods and Model Potentials. John Wiley & Sons, Chichester, 367. https://doi.org/10.1002/047086334X

[68] Wachters, A.J.H. (1970) Gaussian Basis Set for Molecular Wavefunctions Containing Third-Row Atoms. *The Journal of Chemical Physics*, **52**, 1033-1036. https://doi.org/10.1063/1.1673095

[69] Hay, P.J. (1977) Gaussian Basis Sets for Molecular Calculations—Representation of 3D Orbitals in Transition-Metal Atoms. *The Journal of Chemical Physics*, **66**, 4377-4384. https://doi.org/10.1063/1.433731

[70] Raghavachari, K. and Trucks, G.W. (1989) Highly Correlated Systems. Excitation Energies of First Row Transition Metals Sc-Cu. *The Journal of Chemical Physics*, **91**, 1062-1065. https://doi.org/10.1063/1.457230

[71] Binning, R.C. and Curtiss, L.A. (1990) Compact Contracted Basis-Sets for 3rd-Row Atoms: Ga-Kr. *Journal of Computational Chemistry*, **11**, 1206-1216. https://doi.org/10.1002/jcc.540111013

[72] McGrath, M.P. and Radom, L. (1991) Extension of Gaussian-1 (G1) Theory to Bromine-Containing Molecules. *The Journal of Chemical Physics*, **94**, 511-516. https://doi.org/10.1063/1.460367

[73] Curtiss, L.A., McGrath, M.P., Blaudeau, J.-P., Davis, N.E., Binning, R.C. and Radom, L. (1995) Extension of Gaussian-2 Theory to Molecules Containing Third-Row Atoms Ga-Kr. *The Journal of Chemical Physics*, **103**, 6104-6113. https://doi.org/10.1063/1.470438

[74] Dolg, M., Stoll, H., Savin, A. and Preuss, H. (1989) Energy-Adjusted Pseudopotentials for the Rare Earth Elements. *Theoretical Chemistry Accounts*, **75**, 173-194. https://doi.org/10.1007/BF00528565

[75] Küchle, W., Dolg, M., Stoll, H. and Preuss, H. (1994) Energy-Adjusted Pseudopotentials for the Actinides. Parameter Sets and Test Calculations for Thorium and Thorium Monoxide. *The Journal of Chemical Physics*, **100**, 7535. https://doi.org/10.1063/1.466847

[76] Kaupp, M., Schleyer, P.V.R., Stoll, H. and Preuss, H. (1991) Pseudopotential Approaches to Ca, Sr, and Ba Hydrides. Why Are Some Alkaline-Earth MX_2 Compounds Bent? *The Journal of Chemical Physics*, **94**, 1360-1366. https://doi.org/10.1063/1.459993

[77] Andrae, D., Haeussermann. U., Dolg, M., Stoll, H. and Preuss, H. (1990) Energy adjusted ab initio pseudopotentials for the 2nd and 3rd row transition-elements. *Theoretical Chemistry Accounts*, **77**, 123-141.